Analyst

Accepted Manuscript

ROYAL SOCIETY OF CHEMISTRY

www.rsc.org/analyst

Exploring Structure and Formation Mechanism of Amyloid Fibrils by Raman Spectroscopy. A Review.

Dmitry Kurouski[1*], Richard P. Van Duyne[1] and Igor K. Lednev[2]

1. Department of Chemistry, Northwestern University, 2145 Sheridan Road, Evanston, Illinois, USA. E-mail: dkurouski@northwestern.edu
2. Department of Chemistry, University at Albany, State University of New York, 1400 Washington Ave., Albany, USA.

Abstract

Amyloid fibrils are β-sheet rich protein aggregates that are strongly associated with various neurodegenerative diseases. Raman spectroscopy has been broadly utilized to investigate protein aggregation and amyloid fibril formation and has shown to be capable of revealing changes in secondary and tertiary structure at all stages of fibrillation. When coupled with atomic force (AFM) and scanning electron (SEM) microscopies, Raman spectroscopy becomes a powerful spectroscopic approach that can investigate structural organization of amyloid fibril polymorphs. In this review, we discuss the applications of Raman spectroscopy, a unique, label-free and non-destructive technique, for the structural characterization of amyloidogenic proteins, prefibrilar oligomers, and mature fibrils.

Introduction

The rapid aggregation of misfolded proteins is commonly associated with various neurodegenerative diseases, such as Alzheimer disease, Parkinson disease, systematic amyloidosis and type II diabetes.[1, 2] The *post mortem* microscopic examination of organs and tissues of patients diagnosed with these severe maladies reveals amyloid plaques that contain long, unbranched, rod-like protein aggregates, known as amyloid fibrils.[3-5] Amyloid plaques give a positive iodine stain, which is typical for cellulose-containing substances. This observation made Rudolf Virchow conclude that amyloid plaques contain starch. In 1854, he proposed the term 'amyloid', which means 'starch-containing'.[6] Despite the later demonstration by Friedreich and Kekule that proteins, rather than polysaccharides, are the main component of amyloid plaques, the term 'amyloid' continued to be utilized to describe β-sheet rich protein aggregates.[7]

There are several hypotheses on how amyloid fibrils form. One hypothesis suggests that rapid protein aggregation is initiated inside multivesicular bodies.[8] As a result, prefibrilar oligomers are formed. Uncontrollable growth of these aggregates leads to destruction of the cell integrity and a release of fibril species into the extracellular space. The fibril species then propagate into amyloid fibrils. According to the second hypothesis, fibril formation is a defense mechanism that is aimed to isolate highly toxic misfolded proteins and their oligomers from the cell media, by 'packing' them into the much less toxic fibrillar form.[9, 10] *In vitro* studies have revealed that more than 25 proteins can aggregate forming fibrils.[1,5, 11] Protein aggregation typically exhibits a lag phase, followed by a rapid elongation phase, and then an asymptotic phase.[1,12, 13] During the lag phase, soluble prefibrilar oligomers aggregate in multiple assembly states forming a nucleus. The nuclei template protein aggregation causing formation of fibrils.[13-15]

Raman spectroscopy has been broadly used to investigate changes in secondary structure at all stages of protein aggregation and amyloid fibril formation.[16-18] In particular, normal Raman (NR) spectroscopy is commonly used to elucidate conformations of disulfides in both proteins and amyloid fibrils.[19, 20] Coupling of hydrogen-deuterium exchange (H/D exchange) with deep UV Raman (DUVRR) spectroscopy allows one to elucidate fibril core structural organization and determine the psi (Ψ) dihedral angle of the protein backbone. [18,21-23] In addition, DUVRR provides valuable information about the local environment near aromatic amino acids, such as phenylalanine and tyrosine. This can be utilized to monitor the changes in protein secondary structure that occur upon protein aggregation.[14, 24] Recently, the combination of Raman spectroscopy with atomic force microscopy (AFM) or scanning electron microscopy (SEM), has become a powerful analytical approach for investigating the structural organization of fibril polymorphs.[25-27] Fibril polymorphism is a unique phenomenon that occurs when different morphologies and secondary structures from the same protein aggregate at slightly different temperatures, pH values, or other experimental conditions.[27]

Surface-enhanced Raman spectroscopy (SERS) has also been utilized to probe the surface organization of macroscopic objects, such as viruses and amyloid fibrils. SERS is an ultra-sensitive technique that was discovered in 1977 by Jeanmaire and Van Duyne.[28] When a molecule is located within 1-2 nm of a noble metal nanostructure, there is drastic amplification of the Raman signal. It was also demonstrated that the electromagnetic enhancement exponentially decays as the distance from the metal nanostructures increass.[29, 30] This advantage made surface-enhanced Raman spectroscopy a widely used analytical approach for the detection and identification of various analytes, ranging from warfare agents to biomolecules.[31-34] Tip-enhanced Raman Spectroscopy (TERS) combines the sensitivity of SERS and the precise spatial control of scanning probe microscopy (SPM) via a nanometer scale noble metal tip.[35-37] AFM based TERS (AFM-TERS) has been utilized to obtain information about the structural organization of the insulin fibril surface at the nanoscale.[38, 39] Using TERS, information about the amino acid composition of amyloid fibrils and protein secondary structure on their surfaces can be obtained. Furthermore, TERS and SERS spectra acquired from large protein molecules and their aggregates are usually quite different than NR spectra of these species.[35,40]

1. Physical Principles of Raman effect.

Upon the illumination of a molecule with electromagnetic radiation, an exchange of a quantum vibrational energy between the two occurs, resulting in a vibrational frequency difference between the incident and scattered light. This inelastic scattering phenomenon, known as the Raman effect, has been well-described in the litertature.[41-43] The inelastic scattering of photons (Raman scattering) is a very rare event. Only one out of 10^{10} of the incident photons is inelastically scattered.[43] Nevertheless, these photons provide the information about molecular vibrations and consequently structure of the analyzed specimen. In NR scattering, the photon is inelastically scattered with the lower (Stokes scattering) or higher (anti-Stokes scattering) energies, leaving the molecule in the excited vibrational state of the electronic ground state (Figure 1). The same vibrational transition takes place upon resonance Raman scattering with the only difference that the excitation occurs with the frequency of the electronic absorption band. In this case, the vibrational modes, whose motions are coupled to the driven motion of the electronic transition, are primarily observed.

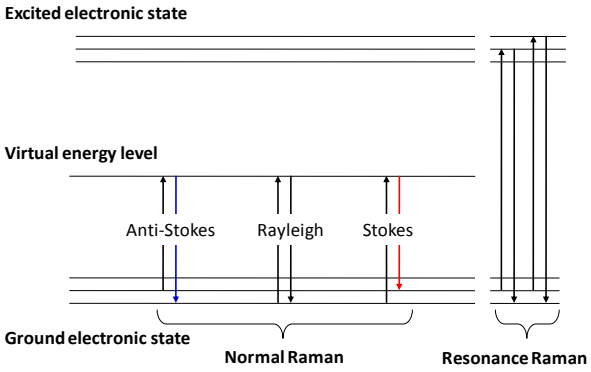

Figure 1. Comparison of NR and Resonance Raman (RR) scattering.

2. Instrumentation.

Confocal Raman spectrometers that are based on either up right on inverted microscopes are commonly used for an acquisition of NR spectra of protein species.[20, 44] Since the Raman cross-section of chemical groups in the typical protein amino acid sequence is relatively small, large protein concentrations (10-100mg/ml) are commonly required to acquire NR spectra of protein species in solution. To avoid overheating and photodegradation, near IR laser excitation is typically used for NR spectroscopy of proteins and protein aggregates.[19,20]

The utilization of different incident radiation frequencies allows for a selective resonance enhancement of a particular region in a protein molecule (resonance Raman).[24, 45, 46] The resonance Raman effect can give a 10^4-10^6 fold signal increase, compared to NR.[43] For example, Tyr and Tpr amino acid bands dominate in the Raman spectrum of protein at ~229 nm excitation.[47] In-plane ring vibrations of heme in heme-containing proteins, such as hemoglobin, can be selectively probed using 415 nm laser radiation (Soret absorption).[48, 49] Deep UV light (195-206 nm) generates Raman spectra dominated by amide chromophore vibrational modes.[45, 50] A Nd:YLF pumped Ti:Sapphire laser is a convenient source for generating light within 193-240 nm range by quadrupling the fundamental frequency of Ti:Sapphire laser radiation. Sample stirring or flowing during measurement is employed to avoid solution overheating and consequently protein photodegradation.[45] Schematic diagrams of typical back-scattering UVRR instruments can be found elsewhere.[18, 45]

3. Interpretation of Raman spectra of protein specimens.

Amide chromophore.

A typical Raman spectrum of a protein is composed of contributions from three major types of vibrational modes, which originate from the polypeptide backbone (amide bands), and from aromatic and non-aromatic amino acid residue side chains. Amide modes include: the amide I vibration (1640-1680 cm^{-1}),

which primarily represents C=O stretching and a small amount of out-of-phase C-N stretching; the amide II vibration (~1550 cm^{-1}), which consists of an out-of-phase combination of C-N stretching and N-H bending motions; and the amide III (1200-1340 cm^{-1}), a complex vibration mode which involves C-N stretching and N-H bending.[18, 24, 51] In DUVRR spectra of proteins, Cα-H (1390 cm^{-1}) and C-H (~1450 cm^{-1}), vibrational modes are commonly observed, which represents Cα-H bending and C-H stretching respectively.[24, 52]

From the set of vibrational bands that comprise the amide chromophores, the amide I band is most commonly used to interpret changes in the protein secondary structure. This is in part due to the overlay of the amide II and amide III bands with the vibrational frequencies of certain stretching modes, such as C-C, C-N and CH_2, that substantially complicates their assignment and interpretation.[53-55] The position of the amide I band depends on the conformation of the polypeptide backbone and intra- and intermolecular hydrogen bonds of the protein specimen. The amide I band (located in the 1665-1680 cm^{-1} range) corresponds to a β-sheet structure, while α-helical protein secondary structure corresponds to the amide I band (located in the 1640-1654 cm^{-1}range) The amide I located in the 1654-1665 cm^{-1} range is typically assigned to unordered or disordered protein secondary structures.[16, 56] There is an ongoing discussion as to whether the amide I band in NR spectra of amyloid aggregates could be utilized to determine β-sheet conformations: parallel *vs* anti-parallel β-sheets.[57-59] Anti-parallel β-sheets have weaker hydrogen bonding compared to parallel β-sheet. Therefore, the amide I band of anti-parallel β-sheet should have higher Raman shift values than the amide I band of parallel β-sheet. Simulations of the anisotropic Raman amide I profiles of anti-parallel and parallel β-sheets demonstrated that the position of the amide I band depends also on the number of strands. A decrease in the number of strands from 12 to 1 causes a large red-shift of the amide I peak for the parallel β-sheet and a negligible peak shift in the case of anti-parallel β-sheet. Measey et al. demonstrated that even a 3° twist and/or a 2° bend per strand could cause a detectible red-shift of amide I band of the parallel β-sheet.[57, 59] This indicates that the amide I position in NR spectra could not be directly utilized for the determination of β-sheet conformations (parallel *vs* anti-parallel) of amyloid fibrils.

The Raman cross-section of the amide II band is very small at near IR (~785 nm) laser excitation, which makes this band invisible in the NR spectra of proteins and fibrils.[20,44] In contrast, the strong amide II band is always evident in DUVRR spectra of proteins and peptides.[18,24,27] The H/D exchange causes a red-shift of the amide II DUVRR band, which is typically called amide II' (~1440 cm^{-1}). This analytical approach is commonly used to determine the amount of 'accessible' protein structure, which can be as attributed to unordered parts of amyloid fibrils. Consequently, it can be used to estimate the amount of hydrophobic fibril core, which is inaccessible to the H/D exchange. For example, amyloid fibrils grown from apo-α-lactolbumin exhibited some degree of H/D exchange: both the amide II and amide II' were observed in their DUVRR spectrum (Figure 2).[19] However, only the amide II' band was observed in the DUVRR spectrum of fibrils formed from apo-α-lactolbumin mutant with the only one out of four disulfides, known as 1-SS-lactolbumin. This indicated that 1-SS-lactolbumin fibrils had no protected hydrophobic core.

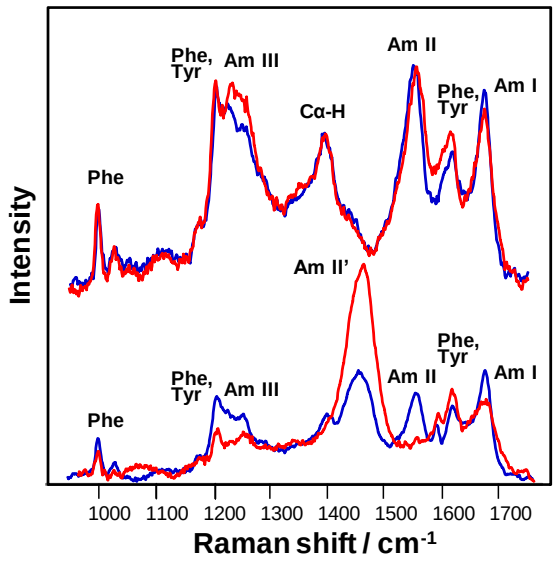

Figure 2. DUVRR spectra of apo-α-lactalbumin (blue) and 1-SS-lactolbumin (red) fibrils in H_2O (top row) and D_2O (bottom row).[19]

The amide III is the most complicated band in the DUVRR spectrum of protein specimens, which consists of three sub-bands: amide III_1, amide III_2 and amide III_3.[18, 51] Asher's group developed a semi-empirical approach that allows for calculating the sci (Ψ) dihedral angle of the polypeptide backbone based on the position of the amide III_3 band.[60, 61] They also found some dependence of the amide III_3 Raman shift on the other, phi (Φ), angle.[62] The analysis of the amide III_3 band can be used to determine the contribution of various secondary structural elements, including PPII and the 2.5_1 helix. For example, the 2.5_1 helix has a characteristic amide III_3 peak at ~1270 cm^{-1}, while amide III of PPII is substantially blue-shifted (~1246 cm^{-1}).[63, 64] Coupling DUVRR with Circular Dichroism (CD) and advanced statistical analysis allows for obtaining a precise quantitative characterization of the secondary structure in the analyzed protein specimens.[23, 65]

Aromatic amino acids.

Based on the presence or absence of certain amino acid side chain Raman bands, as well as its relative intensity of bands in the NR spectrum of proteins of fibrils, valuable information about the local environment of this amino acid can be obtained. For example, it was demonstrated that the intensity of the Phe band can be employed to probe the local environment of this amino acid. Xu et al. investigated the intensity of the Phe ring stretching mode (1000 cm^{-1}) of N-acetyl-L-phenylalanine ethyl ester (ac-Phe-ee) in different ratios of acetonitrile-water solutions.[51] They have demonstrated that the Raman cross-section of this band gradually increased with an increase in acetonitile fraction, reaching a plateau at ~50% acetonitile. It was concluded that the 1000 cm^{-1} Phe ring stretching mode is sensitive to water exposure and therefore can be utilized to probe the local environment of this amino acid. DUVRR spectroscopic studies of lysozyme aggregation revealed that protein fibrillization is strongly associated with a decrease in the intensity of the Phe band.[51, 66] This indicates that the Phe amino acid side chains appear on the surface of the fibril as the result of lysozyme aggregation. The decrease in the intensity of both the Phe and Tyr was observed during insulin aggregation.[20, 27, 59] It was concluded that the local environment of

these amino acids is changed upon protein aggregation in the fibrillar form. It was also shown that changes in the intensity of aromatic amino acid bands in DUVRR spectra can be utilized to study the inhibition of amyloid-β (Aβ) fibrillation. It was reported that the intensities of Phe and Tyr bands increased upon addition of myricetin, which inhibits Aβ aggregation, suggesting that the flavanoid interacts with the peptide's aromatic amino acid residues.[67]

Non-aromatic amino acids. Disulfide bonds.

Disulfide bands (510-545 cm^{-1}) and the S-H (2575 cm^{-1}) band of cysteins are some of the most-studied non-aromatic vibrational bands of protein specimens. NR spectroscopy is commonly used to determine conformations of disulfide bonds in proteins and their aggregates. The Raman shifts of the disulfide bands directly depend on their conformations in the amino acid sequence. Therefore, analysis of these bands becomes extremely valuable for the structural characterization of tertiary and secondary protein structures.[16] Specifically, the gauche-gauche-gauche (g-g-g) conformation has a band at 507 cm^{-1}; the gauche-gauche-trans (g-g-t) has a band at 523 cm^{-1}; and the trans-gauche-trans (t-g-t) has a band at ~545 cm^{-1}. Using NR spectroscopy Kurouski et al. demonstrated that insulin disulfide bond conformations were preserved and do not scramble upon protein aggregation into fibrillar form.[20] This also indicated that disulfides do not break up during insulin fibrillation. Molecular dynamics (MD) simulations that modeled this process confirmed that aggregation of two insulin monomers in a β-sheet rich dimer occurs without the breakage of disulfide bonds. Insulin dimer, which is formed within 15 ns, acts as a template for further protein aggregation, which leads to the formation of insulin fibrils.[20]

It was also shown that disulfide bridges play an important role in the formation of amyloid fibrils *in vitro*. For example, a reduction of disulfide bonds by tris (2-carboxyethyl) phosphine (TCEP) drastically accelerates lysozyme fibrillization, resulting in the formation of more toxic fibril species relative to the fibrils formed from intact protein.[68,69] Kurouski et al. studied aggregation of apo-α-lactoalbumin and its mutant with only one out of four disulfide bonds (1-SS-lactoalbumin). It was found that at low pH these two proteins aggregate forming morphologically different fibril (Figure 3, A). Apo-α-lactoalbumin has four disulfide bonds in g-g-g (510 cm^{-1}), g-g-t (525 cm^{-1}) and t-g-t (535 cm^{-1}) conformations, while the single band of 1-SS-lactoalbumin adopts a t-g-t conformation (Figure 3, B). At the same time, apo-α-lactoalbumin fibrils have exclusively g-g-g conformations (508 cm^{-1}), while 1-SS-lactoalbumin fibrils have no disulfide bonds present (Figure 3, C).[19]

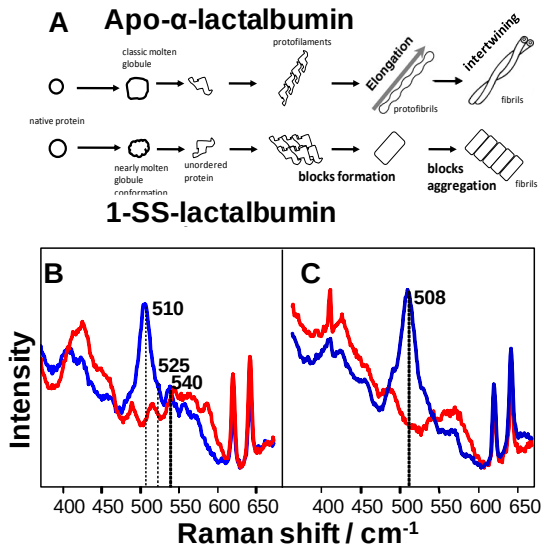

Figure 3. Schematic diagram (A) of apo-α-lactoalbumin and 1-SS-lactoalbumin aggregation pathways. Normal Raman spectra of native (B) apo-α-lactoalbumin (blue) and 1-SS-lactoalbumin (red) proteins and their fibrils (C).

The effect of H_2S on the disulfide bonds of human white egg lysozyme (HEWL) was recently investigated. Rosario-Alomar et al. recently demonstrated that at millimolar concentrations H_2S modifies lysozyme disulfide bonds preventing protein aggregation into toxic amyloid fibrils. Instead, spherical aggregates are formed that exhibit no cell toxicity (Figure 4, A and B). DUVRR spectroscopy revealed that these spherical aggregates have predominantly disordered secondary structure (Figure 4, C). Rosario-Alomar et al. investigated the nature of H_2S interactions with disulfide bonds using NR spectroscopy.[70] It was found that sulfur atom of H_2S becomes endogenously incorporated in protein disulfide bonds, which lead to the formation of trisulfides (SSS).

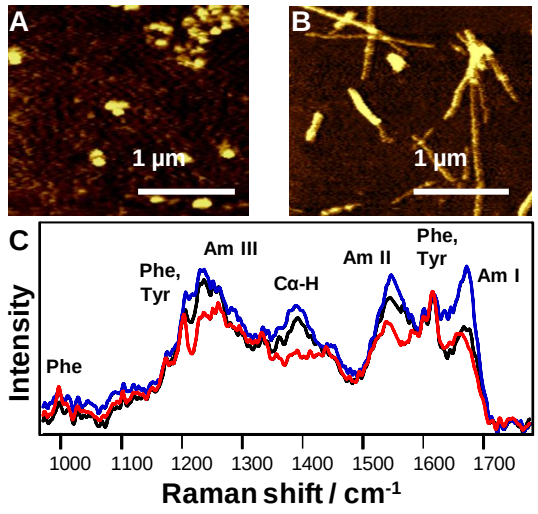

Figure 4. AFM images of HEWL incubated with (A) and without (B) 12 mM of H_2S for 48 hours at 60 °C. DUVRR spectra (C) of native HEWL (red), HEWL fibrils (blue) and spherical aggregates formed in

the presence of H_2S (black); spectra were normalized using the aromatic amino acid Raman band around 1600 cm^{-1} for comparison.

4. Early stages in protein aggregation. Detection of prefibrilar oligomers.

High temperature, ionic strength, and low pH are commonly used to accelerate *in vitro* protein aggregation. During this process, hydrogen bonds that stabilize the native protein conformation break up, which results in the unfolding of the protein amino acid sequence. The free energy of the unfolded protein sequence can be minimized by adopting β-sheet secondary structure.[1,66] As a result, β-sheet-rich oligomers are formed.[15,20] The oligomers aggregate in multiple assembly states forming a nucleus. After a critical concentration of the nuclei is reached, they rapidly propagate into filaments and consequently, fibrils.[13] Prefibrilar oligomers and nuclei are intrinsically instable and present at low sub nanomolar concentrations. This makes their detection and structural characterization extremely challenging. Therefore, very little is known about their structural organization.

Lednev group pioneered the application of two-dimensional correlation spectroscopy (2DCoS) combined with DUVRR spectroscopy.[15] Using 2DCoS and DUVRR Shashilov et al. studied aggregation of HEWL. They found the correlation between the Cα-H band and the amide I band in the DUVRR spectra of HEWL when they compared different time points of the protein aggregation. It was concluded that melting of α-helix caused an appearance of a disordered protein secondary structure. The newly formed β-sheet is consequently developed from this disordered HEWL. Shashilov et al. found that β-sheet rich species, which are formed at early stages of HEWL fibrillations, could not be removed by centrifugation.[15] They also found that the supernatants of HEWL samples incubated for 48h could seed the protein fibrillation, eliminating the lag-phase. Based on this, the authors concluded that the formed β-sheet rich species detected in the supernatants of the incubated samples could be nuclei.[15]

DUVRR spectroscopy was also utilized to investigate insulin aggregation. However, using this technique β-sheet rich prefibrilar species could not be detected.[12] Therefore, Kurouski et al. utilized SERS for the detection of insulin oligomers.[12] To achieve this, sample aliquots were taken at different stages of insulin aggregation at pH 1.6 (65 °C) and centrifuged to remove filaments and short fragments of fibrils. After that, the sample supernatants were mixed with 90 nm Au nanoparticles and analyzed using SERS. It was assumed that insulin dimers and higher molecular weight oligomers had an almost equal adsorption to the gold surface. Since prefibrilar oligomers are β-sheet-rich species, it was assumed that each adsorbed oligomer exhibited a defined "SERS fingerprint," namely the amide I band in 1665–1680 cm region. Kurouski et al. counted the number of SERS spectra containing the amide I band in this spectral region for all sample aliquots that were taken at different stages of insulin aggregation. It was found that the amount of insulin oligomers increased more than twice after the first hour of incubation and then slowly decreased with time. This decrease in the amount of oligomers is kinetically linked to their conversion into fibrils. This study revealed that SERS can be utilized to detect rare protein species such as prefibrilar oligomers. Moreover, information about the secondary structure of these prefibrilar oligomers could be obtained. Kurouski et al. demonstrated that in addition to the sensitive detection, SERS was capable of a semiquantitative estimate of the amount of the oligomers during the different stages of protein aggregation.

Recently, DUVRR spectroscopy was utilized to investigate changes in the secondary structure of Aβ (1-40) peptide in anionic lipid bilayers. It was found that the peptide initially adopts mixtures of disordered

and helical structures upon the interaction with anionic liposomes, which is followed by their conversion into β-sheet over longer time frames.[71]

5. Structural organization of mature amyloid fibrils.

Morphologically different fibrils could grow from the same protein or peptide under slightly different conditions, a phenomenon known as fibril polymorphism.[25, 26, 27, 59] Fibril polymorphism could be caused by variations of monomer-monomer associations at the stage of protein nucleation.[52] Consequently, these nuclei would lead to a formation of structurally and morphologically different fibrils. Alternatively, the deviation of fibril morphology could originate from the differences in the associations of fibril filaments. Specifically, fibril filaments can either braid and coil or associate side-by-side, forming twisted or tape-like fibrils respectively (Figure 5). These morphologically different fibrils will consequently have the same structure.[27, 59, 72, 73]

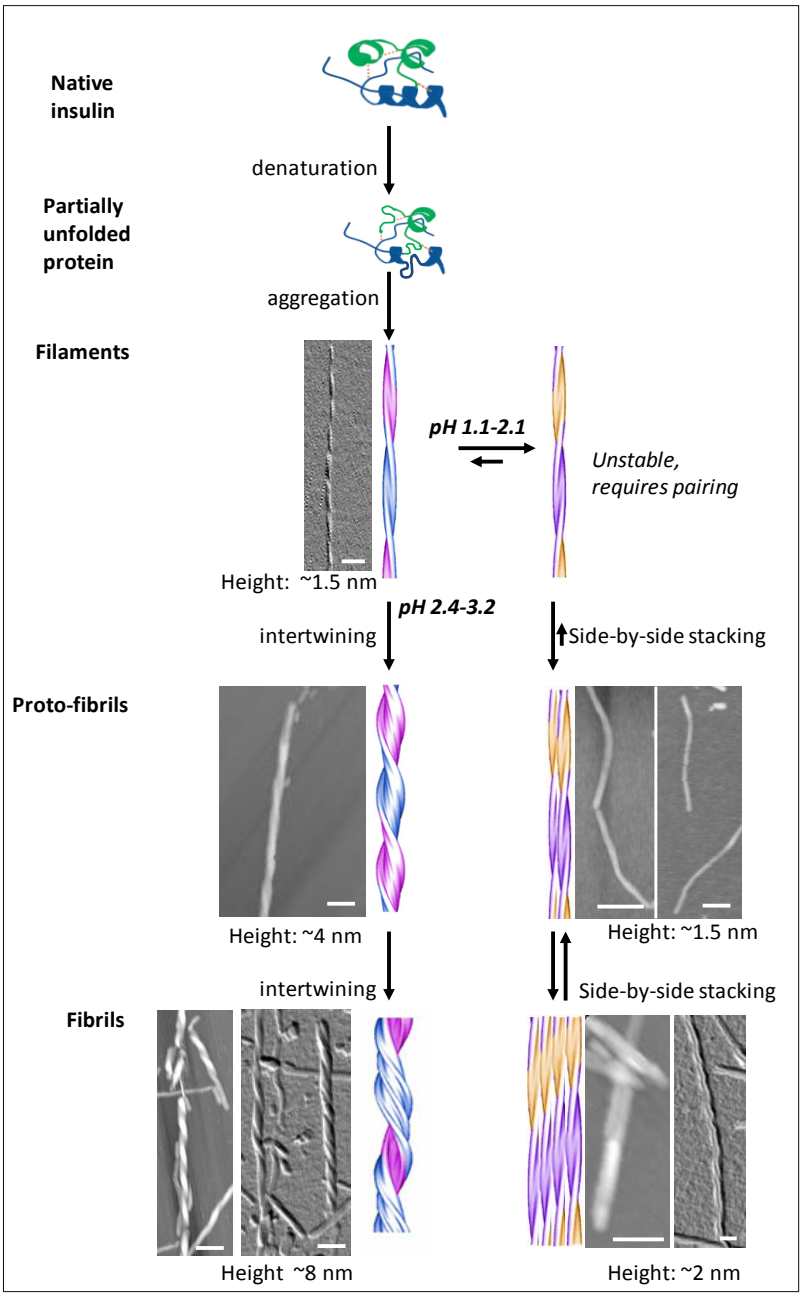

Figure 5. Aggregation of insulin at different pH leads to the formation of twisted or flat fibril polymorphs.

Physical and chemical factors, such as pH, temperature, or salinity, could determine the formation of one or another fibril polymorph.[74, 75, 76] For example, it was found that an aggregation of insulin below pH 2 leads to the formation of tape-like fibrils.[59,72]At the same time, long left-twisted fibrils were observed if the protein was aggregated above pH 2 (Figure 5). DUVRR spectroscopy was used to probe secondary structure of both insulin fibril polymorphs. Kurouski et al. found that DUVRR spectra of both fibril polymorphs exhibited sharp and intense amide I, II, and II bands, as well as Cα-H band (Figure 6, A). Raman shifts and intensities of all amide bands are nearly identical, which indicated that fibril

polymorphs share the same secondary structure. The authors used Asher's semiempirical approach to calculate the Ψ dihedral angle of the fibril cross-β-core, which was found to be equal to 135°. It was also found that Raman bands of Tyr have different intensity in DUVRR spectra of two fibril polymorphs. These authors concluded that Tyr amino acid residues had different local environment in the two fibril polymorphs.[59]

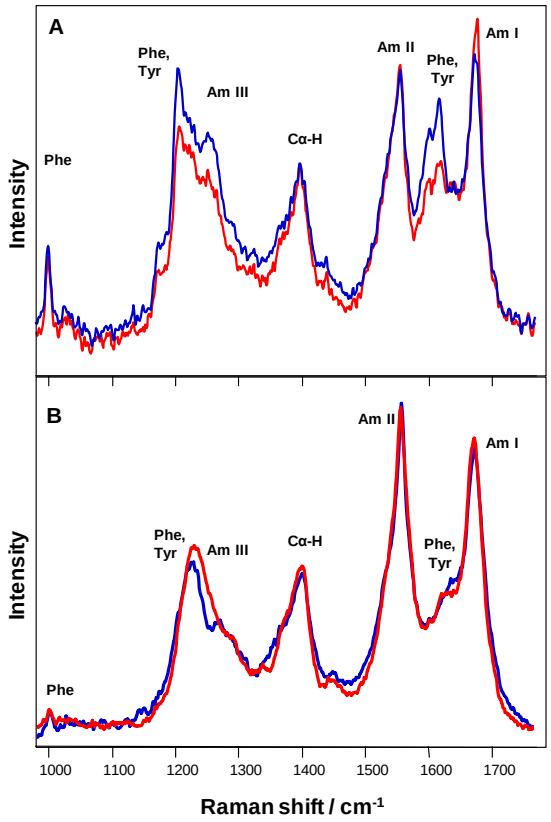

Figure 6. DUVRR spectra of insulin fibrils (A) grown at pH 3.1 (blue), 1.5 (red) and HET-s $_{(218-289)}$ prion fibrils (B) grown in pH 2.0 (red) and 3.9 (blue).

It has been recently shown that pH-controlled fibril polymorphism is a rather general phenomenon, typical for a large group of amyloidogenic proteins and peptides.[27] Using DUVRR spectroscopy, Kurouski et al. investigated protein secondary structure of fibril polymorphs formed from the same protein or peptide under different pHs.[27] It was found that both lysozyme fibril polymorphs and polymorphs formed from a fragment of transthyretin ($TTR_{110-115}$) have the same cross-β core structure. Similar to insulin fibrils, Tyr amino acid residues have different local environments in lysozyme fibril polymorphs. Based on these results, Kurouski et al. concluded that different fibril polymorphs of insulin, lysozyme and a fragment of transthyretin ($TTR_{110-115}$) form either by coiling or side-by-side stacking of their filaments. HET's prion from *Podospora anserina* was demonstrated to form morphologically different fibrils at pH 2.0 and 3.9.[77] DUVRR revealed that positions of the amide I and II bands and C_α-H band are nearly identical in the spectra of both fibril polymorphs. This indicates a high level of similarity of their secondary structures (Figure 6, B). At the same time, HET-s fibrils that were grown at pH 3.9 have substantially higher amount of unordered structure (a peak ~1268 cm^{-1}) than those grown at pH 2.0 fibrils.[27]

Serum amyloid A (SAA) is the main protein component of amyloid fibrils detected in the inflammation-related disease amyloid A (AA) amyloidosis.[78] There are several isoforms of SAA with a high sequence identity, however, not all of them are pathogenic. Srinivasan et al. recently investigated morphologies and structural organization of prefibrilar oligomers and mature fibrils formed from two murine SAA isoforms, named SAA1.1and SAA2.2.[79] It was found that SAA1.1 had an oligomer-rich fibrillation lag phase of a few days, while SAA2.2 formed small fibrils within a few hours, exhibiting virtually no lag phase.[52] DUVRR spectra of the prefibrilar oligomers of both SAA isoforms exhibited identical positions and intensities of the amide bands I, II, and III, indicating that their secondary structure compositions are nearly identical. The amide I band at ~1645 cm^{-1} and the relatively weak Cα—H peak indicated that both SAAs have a predominantly α-helical secondary structure. DUVRR spectra of SAA1.1 and SAA2.2 fibrils showed an increase in the intensity of the amide I and II bands compared with those of refolded proteins, revealing the increase in β-sheet structure. Changes in the shape and intensity of the amide III, CH_2/CH_3, and Cα—H bands were observed in the spectra of SAA2.2 fibrils compared with the refolded protein, suggesting that SAA2.2 undergoes substantial change in polypeptide backbone conformation upon fibril formation. In contrast, changes in the shape and intensity of CH_2/CH_3 and Cα-H bands were less evident for SAA1.1, suggesting that the formation of SAA1.1 fibrils involves much less perturbation of the protein secondary structure (Figure 7). Using AFM, Srinivasan et al. demonstrated that SAA 2.2 oligomers form worm-like proto-fibrils that braid and coil forming twisted fibrils. At the same time, SAA 1.1 oligomers associate into rod-like protofibrils that tend to stack side-by-side forming tape-like fibrils.[52]

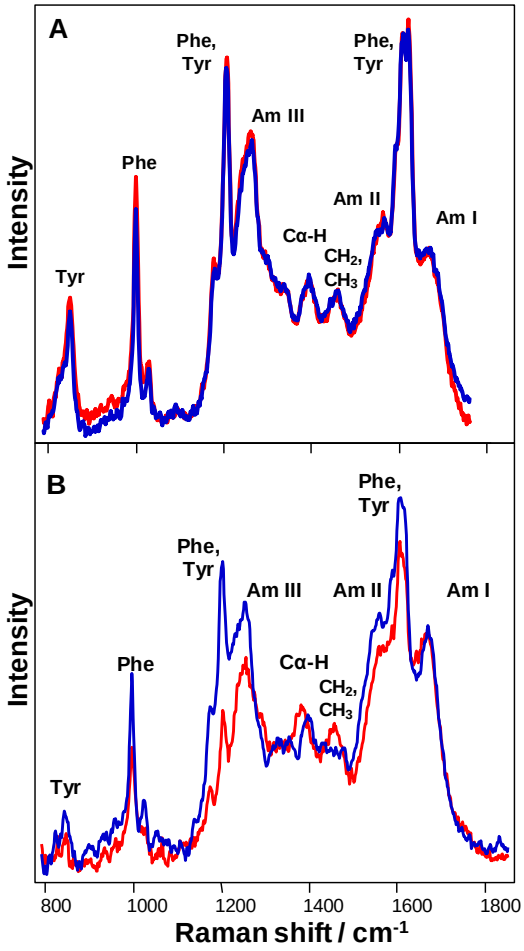

Figure 7. DUVRR spectra of native SAA1.1and SAA2.2 (A) and mature fibrils (B).

The works described above have demonstrated how microscopic techniques, such as AFM or SEM, and DUVRR spectroscopy can be complimentary in the investigation of protein aggregation and fibril polymorphism.

6. Polyglutamine (polyQ) aggregates.

DUVRR spectroscopy and CD were recently utilized to monitor conformation changes of a backbone and side chain residues of a short, polyglutamine (polyGln or polyQ) peptide.[80] PolyQ aggregates are a hallmark of several severe neurodegenerative diseases, such as Huntington disease. Inheritance of an expanded polyQ sequence above a pathological threshold that is associated with a high risk of the disease. It was found that Q10 peptide adopted a β-sheet conformation upon salvation in water. In this conformation, Gln side chains formed hydrogen bonds to either the backbone or other Gln side chains. At 60 °C, Q10 rapidly aggregated, forming amyloid fibrils. If these fibrils are disaggregated, newly formed Q10 monomers adopted PPII-like and 2.5(1)-helix conformations, where the Gln side chains form hydrogen bonds with water. Xiong et al. demonstrated that these newly formed Q10 monomers did not form fibrils unless seeded with the β-sheet conformation of Q10. It was proposed that this is due to high differences between activation barriers of PPII-like/2.5(1)-helix and β-sheet conformations of Q10.

Secondary structure of polyQ aggregates formed from monomers with different length of Gln repeats was recently studied using DUVRR spectroscopy coupled to H/D exchange.[81] Kurouski et al. found that the intensity of both amide II' bands after exchange was substantially higher in the DUVRR spectra of Q41 fibrils comparing to the ones of Q26. This observation suggested that H/D exchange is taking place more extensively in Q41 fibrils than in Q26 fibrils, indicating that fibril core of Q41 fibrils is less protected than the core of Q26 fibrils (Figure 8). Kurouski et al. proposed that filaments of Q41 fibrils could have a higher degree of helical twist, away from planarity, in their β-sheet core structure compared to that of Q26. Such a helical twist would result in weakening the β-sheet hydrogen bonds, allowing much larger degree of the H/D exchange. The increase in helical twist angle, on the order of a few degrees or less per Q residue, over a large supramolecular structure could be significant in terms of Vibrational Circular Dichroism (VCD) intensity enhancement. Indeed, it was found that Q41 fibrils exhibit approximately 10-fold enhancement of the same VCD spectrum compared to the already enhanced VCD of fibrils formed from Gln repeats 30 and below ($Q \leqslant 30$).[81]

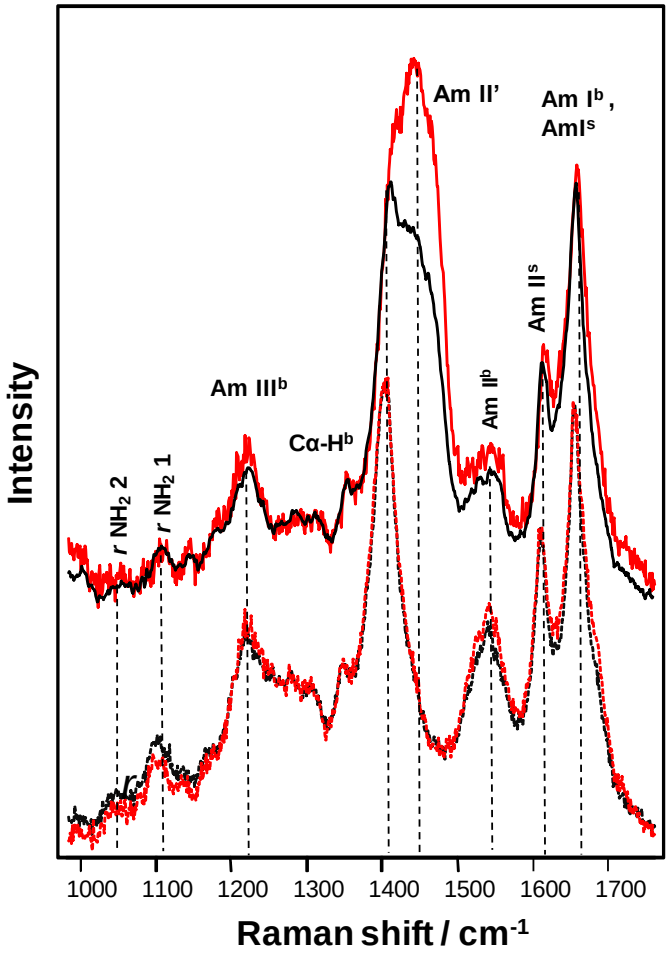

Figure 8. DUVRR spectra of Q41 aggregates (red) and Q26 aggregates (black) in water (dashed lines) and D_2O (solid lines). Subscripts b and s stand for backbone and side chain, respectively.

7. Inter-conversions of fibril polymorphs.

Amyloid fibrils formed from full-length proteins are considered to be the most thermodynamically stable form of proteins. Therefore it was expected that only harsh denaturing conditions such as high pH and pressure or low temperature could disintegrate or deform them. Consequently, no newly formed fibril polymorphs were expected to appear as a result of such perturbations. It was recently demonstrated that fibrils grown from apo-α-lactalbumin in 150 mM NaCl at 37 °C (Polymorph I) change their secondary structure after temperature and ionic strength of the solution were changed.[82] Both 12 °C temperature drop and salt removal were necessary to initiate the fibril structural transformations. One can hypothesize that the osmotic pressure of salt ions trapped in the unordered part of the fibrils plays a role in decreasing the fibril stability while a small temperature drop initiates the swelling of Polymorph I unordered parts. The phenomenon when a small temperature drop initiates significant changes in protein structure,[83] well known as cold denaturation,[84] is thought to be associated with the hydration of the polypeptide chain.[85] The swelling might increase the flexibility of the polypeptide chain and allow for creating hydrophobic pockets. As a result, the local environments of both Trp (based on fluorescence data) and Phe (based on Raman data) became more hydrophobic when the fibrils are swollen and more hydrophilic in the compact fibrils. Refolding of β-sheet occurred at the same time or with some delay as the unordered part collapsed. It is interesting that one type of β-sheet (with a characteristic Amide III_3 Raman peak at 1253 cm^{-1}) only was growing during the refolding process. It is reasonable to assume that the residual of this type of β-sheet "templated" the refolding process. As a result, the structure of the fibril cross-β core is more uniform in Polymorph II than that in Polymorph I.[82]

Shammas et. al. demonstrated that stability of insulin fibrils can be pertrubated through alteration of electrostatic interactions.[86] It was demonstrated that strong electrostatic repulsion could be sufficient to disrupt the hydrogen-bonded cross-β-core, which ultimately resulted in fibril dissociation. Separately, Kurouski et al. demonstrated that a small change in pH drastically changes morphology and supramolecular chirality of insulin fibrils.[87] This process is irreversible and occurs only when the pH is raised from 1.5 to 2.5. No effect of solution ionic strength was found. An addition of sodium chloride up to 1 M concentration to pH 1.5 fibrils did not change the kinetics of the polymorphs' inter-conversion. DUVRR spectroscopy revealed that this process undergoes without a structural reorganization of the fibril cross-β-core. The major changes in the DUVRR spectra of two fibril polymorphs are associated with the intensity of aromatic amino acid residue peaks (Figure 9). Specifically, tyrosine (Tyr) bands in the spectrum of insulin fibrils that were formed as a result of pH elevation have significantly higher intensity than in the spectrum of initial fibril polymorph grown at pH 1.5. It points to the difference in Tyr local environments in these two fibril polymorphs. At the same time, the intensity of phenylalanine (Phe) peak at 1000 cm^{-1} did not change as a result of polymorphs' inter-conversion. Authors proposed that Tyr residues are located on the surface of two proto-fibrils, which were formed as a result of pH 1.5 fibril disintegration. In contrast, Phe residues are buried inside proto-fibrils and the disintegration of pH 1.5 fibrils does not change their local environment.

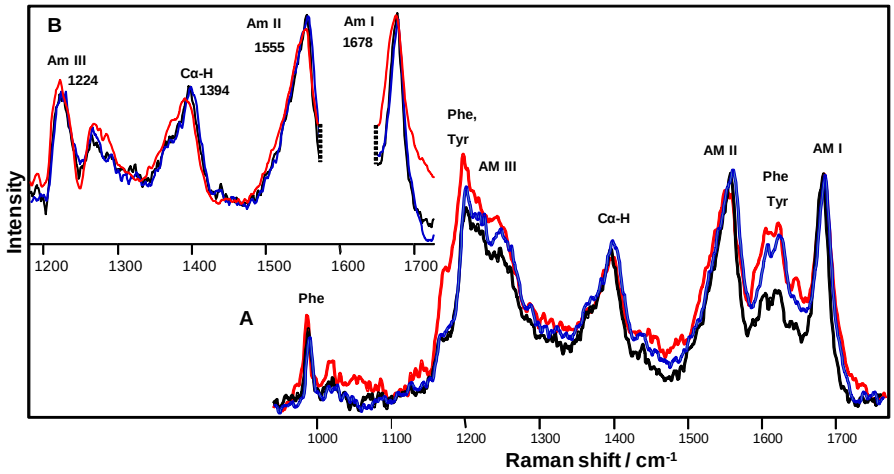

Figure 9. DUVRR spectra insulin fibrils grown at pH 1.5 (black), the same solution of pH 1.5 insulin fibrils after 30 min at pH 2.5 (red), insulin fibrils grown at pH 2.5 (blue). The same spectra (B) after quantitative subtraction of Phe and Tyr contribution.

8. Polarized Raman spectroscopy of insulin fibrils.

Polarized Raman spectroscopy offers a unique opportunity in structural characterization of anisotropic samples, such as amyloid fibrils. This methodology is based on the measurement of the change in intensity of a particular Raman band, as a function of the angle between the incident laser polarization and the fibril axis. Polarization characteristics of Raman scattering are related to the polarizability tensors and therefore carry symmetry information of the chemical groups. It was shown that if the Raman tensor of a chemical group is known, its orientation in the protein aggregates can be obtained.[88-90] Sereda and Lednev have recently applied polarized Raman spectroscopy to investigate the orientation of peptide bond carbonyls (the amide I band) in insulin fibrils.[91] The largest intensity of the amide I band was observed if the main fibril axis was co-linear with the direction of the electric field component of the polarized laser radiation.[91] It was found that the intensity of the amide I decreased more than five fold when the sample was rotated from 0° to 90°, retaining only 18% of its maximum intensity. The results indicated that carbonyl groups have almost parallel orientation (13 ± 5°) relative to the main axis of the fibril. In addition to amide I, vibrational bands at 643, 830 and 1616 cm^{-1}, which could be assigned to the phenoxyl ring of tyrosine, exhibited polarization-dependent intensity changes. It was predicted that the average orientation of the tyrosine phenoxyl ring planes is perpendicular to the main fibril axis.

9. Tip-Enhanced Raman Spectroscopy (TERS) uniquely probes the surface of fibrils.

NR and DUVRR spectroscopy probe the whole volume of the fibril, while TERS is capable of providing structural information about the fibril surface. TERS combines the high sensitivity of SERS and the precise spatial control and resolution of scanning probe microscopy (SPM) via a nanometer scale noble metal scanning tip.[36, 92-94] Two forms of SPM include scanning tunneling microscopy (STM) and atomic force microscopy (AFM).[37, 38, 92, 95]The substrate generality of TERS has already been utilized to investigate various topics in biological and surface chemistry such as detecting cytochrome c oxidation in

mitochondria,[96] monitoring catalytic reactions,[97] imaging mixed polymer surfaces,[98] and single-wall carbon nanotubes.[99] Furthermore, single-molecule detection has been achieved using TERS.[100-102]

Interpretation of TER spectra from protein specimens is quite complicated. There are vibrational modes that could be related to more than one amino acid or chemical group. For example, CH, CH_2 and CH_3 bands (1475 cm^{-1}, 1457 cm^{-1}, 1372-1377 cm^{-1}, 1355 cm^{-1}) could originate from alanine, valine, leucine, and isoleucine. Therefore, it is challenging to distinguish amino acid residues with saturated hydrocarbon side chains. Raman band at 1144 cm^{-1} represents the vibrations of amino and imino groups and can be assigned to asparagine, glutamine, lysine and arginine or N terminal amino acid of the peptide chain. Carboxyl groups have two vibrational frequencies at 1400 cm^{-1} and 1687 cm^{-1}. In TER spectra of protein specimens these bands can be assigned to aspartic or glutamic acids, as well as C terminal amino acid of the peptide chain. Nevertheless, aromatic amino acids Tyr, Phe and hisitidine (His) have clearly defined Raman bands and therefore can be unambiguously assigned. Utilization of silicon or silicon nitrile cantilevers in AFM-TERS instruments obscures the visualization of disulfide bands (510-540 cm^{-1}) that overlap with the Raman band of the silicon (521 cm^{-1}). Nevertheless, C-S vibrations of cysteins (Cys) (650-690 cm^{-1}, 750-790 cm^{-1} and 800 cm^{-1}) can be clearly resolved. Based on the presence or absence of cysteine bands valuable information about localization of disulfide bridges on the surface of protein specimens can be obtained.

In addition to the amino acid composition, TERS can resolve protein secondary structure of the protein specimens. It was shown that both amide I and amide III bands can be used to interpret protein secondary structure.[38, 103, 104] The interpretation of amide I band (1640-1680 cm^{-1}) is relatively straightforward because there are no amino acid bands present in this spectra region.[35, 38, 104] However, assignment of vibrational bands in amide III region (1200-1340 cm^{-1}) to the protein chromophore is rather challenging due to vibrational bands of some chemical groups (CC ring, COH and CH_2) that can be found at these Raman shifts.

Finally, several research groups have reported that vibrational bands in TER spectra can shift on approximately +/-7 cm^{-1} relative to their corresponding bands in NR spectra.[92, 104] The origin of these band fluctuations is not yet clear. It was proposed that such band shifts could be due to molecule-metal interactions and incident light polarization.[40, 104, 105, 106]

In the last decade TERS was intensively used to characterize structural organization of amyloid fibrils. Deckert-Gaudig et al. demonstrated that selected amino acids and changes in the secondary structure, namely α-helix, β-sheet, could be probed with a lateral resolution better than 2 nm.[103] TERS spectra were collected along a 12 nm profile on the fibril with a 0.5 nm steps. The acquired spectra demonstrate changes in the selected amino acids over the entire examined area. Specifically, the intensity of His bands substantially increased only in three TER spectra collected on one side of the fibril. This indicated that tip was approaching His amino acid residue on the fibril surface. Proline (Pro), a rare amino acid in the insulin sequence (1 out of 51 residues) was observed only in two of the acquired spectra, suggesting that the single amino acid side chain can be resolved using TERS.

Using TERS, Kurouski at al. demonstrated a correlation between some amino acids and protein secondary structure on the fibril surface.[38] It was found that aromatic amino acids, such as Tyr and Phe, as well as

Cys were much more frequently present on β-sheet clusters than on the areas with α-helix/ unordered protein secondary structure. Pro amino acid on the opposite, was much more abundant in clusters with α-helix/ unordered protein. TERS was also used to investigate surface organization of insulin fibril polymorphs with different topologies: flat, tape like and twisted.[39] It was found that surfaces of these polymorphs have distinctively different amino acid composition and protein secondary structures. It should be noted that for the first time the surface of filaments, precursors of fibril, was characterized. Comparison of the amino acid propensities and protein secondary structures on the surface of the filaments with those on the surfaces of mature fibrils allowed the authors to propose a hypothetical mechanism of filaments' propagation into mature insulin fibrils.[39]

Paulite et al. utilized TERS to image nanotapes formed from β-Amyloid (1–40) peptide fragments.[107] Authors plotted the intensity of Phe band at each pixel location and obtained TERS map was then compared to the corresponding topographic images. It was shown that features, such as small areas of nanotapes, which were not evident in topographic images, could be visualized by TERS (Figure 10). At the same time, the reported TERS spectra were practically lacking other vibrational bands. The origin of such a difference between the intensity of Phe ring mode and other vibrational bands in TERS spectra is unclear. Inter-laboratory study of CysPhePhe demonstrated that indeed only a few of the peptide vibrational modes (including Phe ring mode) visible in NR can be detected using TERS.[108] It should be noted that all reported TERS spectra of CysPhePhe were acquired using STM-TERS instruments. Additional experiments are required to compare AFM- and STM-TERS performances for the characterization of protein specimens.

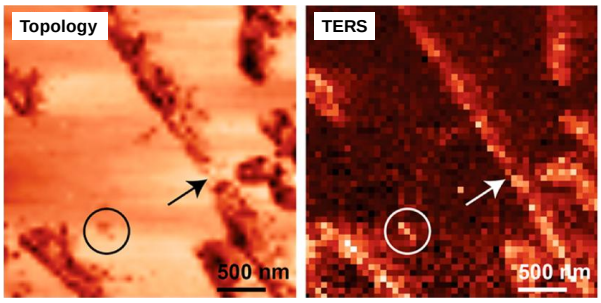

Figure 10. Simultaneously acquired (a) STM and (b) TERS images of individual nanotapes of β-Amyloid (1–40) peptide fragments. The color-coded TERS images display the intensity (high intensity is represented by a brighter pixel) of the aromatic ring breathing marker band (1004 cm^{-1}). The arrow and circle illustrate that areas weakly observed as a feature in the STM image can be identified as nanotape/peptide structures using TERS imaging.

These studies demonstrate a high potential of TERS for the surface characterization of amyloid fibrils. At the same time, they show how challenging is the spectral interpretation of TERS spectra that are collected from specimens with sophisticated chemical composition. Surface imaging at the nanoscale can provide valuable information about toxicity of amyloids, as well as shed a light on their aggregation pathways.

Conclusions

Raman spectroscopy, including DUVRR, SERS and TERS, is a powerful tool for structural characterization of protein aggregation and amyloid fibril formation. In this review we have shown that

Raman spectroscopy can be used to reveal mechanisms of protein aggregation and amyloid fibril formation. Together with AFM and SEM, Raman spectroscopy is a powerful spectroscopic approach for structural characterization of amyloid fibril polymorphs. These findings can aid in screening of new drugs that can slow down progression or prevent development of various neurodegenerative diseases associated with protein misfolding.

Acknowledgments

This work was supported in part by the National Science Foundation under Award CHE-1152752 (I.K.L.). We are grateful to Nolan Wong, Michael Mattei and Nilam C. Shah for helpful discussions.

Literature

1. T. P. Knowles, M. Vendruscolo and C. M. Dobson, *Nat. Rev.*, 2014, **15**, 384-396.
2. J. D. Sipe and A. S. Cohen, *J. Struct. Biol.*, 2000, **130**, 88-98.
3. C. M. Wischik, R. A. Crowther, M. Stewart and M. Roth, *J. Cell. Biol.*, 1985, **100**, 1905-1912.
4. C. M. Wischik, M. Novak, H. C. Thogersen, P. C. Edwards, M. J. Runswick, R. Jakes, J. E. Walker, C. Milstein, M. Roth and A. Klug, *Proc. Nat. Acad. Sci. U.S.A.*, 1988, **85**, 4506-4510.
5. R. N. Rambaran and L. C. Serpell, *Prion*, 2008, **2**, 112-117.
6. R. Virchow, *Virchows Arch. Pathol. Anat.*, 1854, **6**, 416-426.
7. N. Friedreich and A. Kekule, *Virchows Arch. Pathol. Anat.*, 1859, **16**, 50-65.
8. R. P. Friedrich, K. Tepper, R. Ronicke, M. Soom, M. Westermann, K. Reymann, C. Kaether and M. Fandrich, *Proc. Nat. Acad. Sci. U.S.A.*, **107**, 1942-1947.
9. C. J. Kay, *FEBS Lett.*, 1997, **403**, 230-235.
10. D. Pogocki, *Acta Neur. Exp.*, 2003, **63**, 131-145.
11. C. M. Dobson, *Nature*, 2003, **426**, 884-890.
12. D. Kurouski, M. Sorci, T. Postiglione, G. Belfort and I. K. Lednev, *Biotechnol. Progr.*, 2014, **30**, 488-495.
13. M. Sorci, R. A. Grassucci, I. Hahn, J. Frank and G. Belfort, *Proteins*, 2009, **77**, 62-73.
14. V. A. Shashilov and I. K. Lednev, *J. Am. Chem. Sci.*, 2008, **130**, 309-317.
15. V. Shashilov, M. Xu, V. V. Ermolenkov, L. Fredriksen and I. K. Lednev, *J. Am. Chem. Sci.*, 2007, **129**, 6972-6973.
16. P. R. Carey, *Biochemical Applications of Raman and Resonance Raman Spectroscopies*, Academ. Press, New York, 1982.
17. J. Dong, Z. Wan, M. Popov, P. R. Carey and M. A. Weiss, *J. Mol. Biol.*, 2003, **330**, 431-442.
18. S. A. Oladepo, K. Xiong, Z. Hong, S. A. Asher, J. Handen and I. K. Lednev, *Chem. Rev.*, 2012, **112**, 2604-2628.
19. D. Kurouski and I. K. Lednev, *Int. J. Biomed. Nanosci. Nanotech.*, 2011, **2**, 167-176.
20. D. Kurouski, J. Washington, M. Ozbil, R. Prabhakar, A. Shekhtman and I. K. Lednev, *PloS one*, 2012, **7**, e36989.
21. M. Xu, V. Shashilov and I. K. Lednev, *J. Am. Chem. Sci.*, 2007, **129**, 11002-11003.
22. V. A. Shashilov and I. K. Lednev, *Chem. Rev.*, 2010, **110**, 5692-5713.
23. V. A. Shashilov, V. Sikirzhytski, L. A. Popova and I. K. Lednev, *Methods*, 2010, **52**, 23-37.
24. I. K. Lednev, in *Protein Structures, Methods in Protein Structures and Stability Analysis*, eds. V. N. Uversky and E. A. Permyakov, Nova Sci., 2007, pp. 1-26.
25. M. Anderson, O. V. Bocharova, N. Makarava, L. Breydo, V. V. Salnikov and I. V. Baskakov, *J. Mol. Cell. Biol.*, 2006, **358**, 580-596.
26. M. Fandrich, *Cell. Mol. Life Sci.*, 2007, **64**, 2066-2078.

27. D. Kurouski, X. Lu, L. Popova, W. Wan, M. Shanmugasundaram, G. Stubbs, R. K. Dukor, I. K. Lednev and L. A. Nafie, *J. Am. Chem. Soc.*, 2014, **136**, 2302-2312.
28. R. P. Van Duyne and D. L. Jeanmaire, *J. Electroanal. Chem.*, 1977, **84**, 1-20.
29. P. L. Stiles, J. A. Dieringer, N. C. Shah and R. P. Van Duyne, *Ann. Rev. Anal. Chem.*, 2008, **1**, 601-626.
30. N. G. Greeneltch, M. G. Blaber, A. I. Henry, G. C. Schatz and R. P. Van Duyne, *Anal. Chem.*, 2013, **85**, 2297-2303.
31. D. Kurouski and R. P. Van Duyne, *Anal. Chem.*, 2015, **87**, 2901-2906.
32. J. F. Betz, W. W. Yu, Y. Cheng, I. M. White and G. W. Rubloff, *Phys. Chem. Chem. Phys.*, 2014, **16**, 2224-2239.
33. S. L. Kleinman, R. R. Frontiera, A. I. Henry, J. A. Dieringer and R. P. Van Duyne, *Phys. Chem. Chem. Phys.*, 2013, **15**, 21-36.
34. E. Ringe, J. Zhang, M. R. Langille, C. A. Mirkin, L. D. Marks and R. P. Van Duyne, *Nanotechnology*, 2012, **23**, 444005.
35. D. Kurouski, T. Postiglione, T. Deckert-Gaudig, V. Deckert and I. K. Lednev, *Analyst*, 2013, **138**, 1665-1673.
36. L. Opilik, T. Bauer, T. Schmid, J. Stadler and R. Zenobi, *Phys. Chem. Chem. Phys.*, **13**, 9978-9981.
37. N. Jiang, E. T. Foley, J. M. Klingsporn, M. D. Sonntag, N. A. Valley, J. A. Dieringer, T. Seideman, G. C. Schatz, M. C. Hersam and R. P. Van Duyne, *Nano Lett.*, **12**, 5061-5067.
38. D. Kurouski, T. Deckert-Gaudig, V. Deckert and I. K. Lednev, *J. Am. Chem. Soc.*, 2012, **134**, 13323-13329.
39. D. Kurouski, T. Deckert-Gaudig, V. Deckert and I. K. Lednev, *Biophys. J.*, 2014, **106**, 263-271.
40. C. Blum, T. Schmid, L. Opilik, N. Metanis, S. Weidmann and R. Zenobi, *J. Phys. Chem. C.* 2012, **116**, 23061–23066.
41. D. A. Long, *The Raman Effect: A unified treatment of the theory of raman scattering by molecules*, West Sussex, England, 2002.
42. P. A. M. Dirac, *Proc. R. Soc. A*, 1927, **114**, 243-265.
43. R. McCreery, *Raman Spectroscopy for Chemical Analysis*, Whiley, New York, 2000.
44. C. Ortiz, D. Zhang, A. E. Ribbe, Y. Xie and D. Ben-Amotz, *Biophys. Chem.*, 2007, **128**, 150-155.
45. I. K. Lednev, V. V. Ermolenkov, W. He and M. Xu, *Anal. Bioanal. Chem.*, 2005, **381**, 431-437.
46. S. A. Asher, *Anal. Chem.*, 1993, **65**, 201A-210A.
47. Z. Ahmed, I. A. Beta, A. V. Mikhonin and S. A. Asher, *J. Am. Chem. Soc.*, 2005, **127**, 10943-10950.
48. G. Balakrishnan, Y. Hu and T. G. Spiro, *Appl. Spectr.*, 2006, **60**, 347-351.
49. G. B. Ray, R. A. Copeland, C. P. Lee and T. G. Spiro, *Biochemistry*, 1990, **29**, 3208-3213.
50. Z. H. Chi and S. A. Asher, *Biochemistry*, 1998, **37**, 2865-2872.
51. M. Xu, V. V. Ermolenkov, V. N. Uversky and I. K. Lednev, *J. Biophoton.*, 2008, **1**, 215-229.
52. S. Srinivasan, S. Patke, Y. Wang, Z. Ye, J. Litt, S. K. Srivastava, M. M. Lopez, D. Kurouski, I. K. Lednev, R. S. Kane and W. Colon, *J. Biol. Chem.*, 2013, **288**, 2744-2755.
53. Z. Movasaghi, S. Rehman and I. U. Rehman, *Appl. Spectr. Reviews*, 2007, **42**, 493-541.
54. S. Stewart and P. M. Fredericks, *Spectrochim. Acta A.*, 1999, **55**, 1641-1660.
55. S. Stewart and P. M. Fredericks, *Spectrochim. Acta A.*, 1999, **55**, 1615-1640.
56. H. Fabian and P. Anzenbacher, *Vibrat. Spectr.*, 1993, **4**, 125-148.
57. R. Schweitzer-Stenner, *J. Phys. Chem.*, 2012, **116**, 4141-4153.
58. T. J. Measey and R. Schweitzer-Stenner, *J. Am. Chem. Soc.*, 2006, **128**, 13324-13325.
59. D. Kurouski, R. A. Lombardi, R. K. Dukor, I. K. Lednev and L. A. Nafie, *Chem. Commun.,* 2010, **46**, 7154-7156.

60. S. A. Asher, A. Ianoul, G. Mix, M. N. Boyden, A. Karnoup, M. Diem and R. Schweitzer-Stenner, *J. Am. Chem. Soc.*, 2001, **123**, 11775-11781.
61. A. V. Mikhonin, S. V. Bykov, N. S. Myshakina and S. A. Asher, *J. Phys. Chem.*, 2006, **110**, 1928-1943.
62. A. Ianoul, M. N. Boyden and S. A. Asher, *J. Am. Chem. Soc.*, 2001, **123**, 7433-7434.
63. C. B. McDonald, V. Bhat, D. Kurouski, D. C. Mikles, B. J. Deegan, K. L. Seldeen, I. K. Lednev and A. Farooq, *Biophys. Chem.*, 2013, **175-176**, 54-62.
64. I. K. Lednev, V. V. Ermolenkov, S. Higashiya, L. A. Popova, N. I. Topilina and J. T. Welch, *Biophys. J.*, 2006, **91**, 3805-3818.
65. O. O. Oshokoya, C. A. Roach and R. D. Jiji, *Anal. Methods*, 2014, **6**, 1691-1699.
66. M. Xu, V. V. Ermolenkov, W. He, V. N. Uversky and I. K. Lednev, *Biopolymers*, 2005, **79**, 58-61.
67. M. Wang and R. D. Jiji, *Biophys. Chem.*, 2011, **158**, 96-103.
68. M. F. Mossuto, B. Bolognesi, B. Guixer, A. Dhulesia, F. Agostini, J. R. Kumita, G. G. Tartaglia, M. Dumoulin, C. M. Dobson and X. Salvatella, *Angew. Chem. Int. Ed.* 2011, **50**, 7048-7051.
69. C. David, S. Foley and M. Enescu, *Phys. Chem. Chem. Phys.*, 2009, **11**, 2532-2542.
70. M. F. Rosario-Alomar, T. Quiñones-Ruiz, D. Kurouski, V. Sereda, E. B. Ferreira, L. D. Jesús-Kim, S. Hernández-Rivera, D. V. Zagorevski, J. López-Garriga, I. K. Lednev, *J. Phys. Chem B.*, 2015, **119**, 1265-1274.
71. J. Xiong, C. A. Roach, O. O. Oshokoya, R. P. Schroell, R. A. Yakubu, M. K. Eagleburger, J. W. Cooley and R. D. Jiji, *Biochemistry*, 2014, **53**, 3004-3011.
72. D. Kurouski, R. K. Dukor, X. Lu, L. A. Nafie and I. K. Lednev, *Biophys. J.*, 2012, **103**, 522-531.
73. V. Shashilov, M. Xu, N. Makarava, R. Savtchenko, I. V. Baskakov and I. K. Lednev, *J. Phys. Chem. B*, 2012, **116**, 7926-7930.
74. J. Adamcik, J. M. Jung, J. Flakowski, P. De Los Rios, G. Dietler and R. Mezzenga, *Nat. Nanotech.*, 2010, **5**, 423-428.
75. T. Härd, *J. Phys. Chem. Lett.*, 2014, **5**, 607-614.
76. C. L. Heldt, D. Kurouski, M. Sorci, E. Grafeld, I. K. Lednev and G. Belfort, *Biophys. J.*, 2011, **100**, 2792-2800.
77. A. Sen, U. Baxa, M. N. Simon, J. S. Wall, R. Sabate, S. J. Saupe and A. C. Steven, *J. Biol. Chem.*, 2007, **282**, 5545-5550.
78. E. Malle, S. Sodin-Semrl and A. Kovacevic, *Cell. Mol. Life. Sci.*, 2009, **66**, 9-26.
79. J. Yu, H. Zhu, J. T. Guo, F. C. de Beer and M. S. Kindy, *Lab. Invest.*, 2000, **80**, 1797-1806.
80. K. Xiong, D. Punihaole and S. A. Asher, *Biochemistry*, 2012, **51**, 5822-5830.
81. D. Kurouski, K. Kar, R. Wetzel, R. K. Dukor, I. K. Lednev and L. A. Nafie, *FEBS Lett.*, 2013, **587**, 1638-1643.
82. D. Kurouski, W. Lauro and I. K. Lednev, *Chem. Commun.*, 2010, **46**, 4249-4251.
83. M. Hansen, M. H. Jensen, K. Sneppen and G. Zocchi, *Europ. Phys. J. B*, 1999, **10**, 193-196.
84. P. L. Privalov, *Crit. Rev. Biochem. Mol. Biol.*, 1990, **25**, 281-305.
85. C. L. Dias, T. Ala-Nissila, M. Karttunen, I. Vattulainen and M. Grant, *Phys. Rev. Lett.*, 2008, **100**, 118101.
86. S. L. Shammas, T. P. Knowles, A. J. Baldwin, C. E. Macphee, M. E. Welland, C. M. Dobson and G. L. Devlin, *Biophys. J.*, 2011, **100**, 2783-2791.
87. D. Kurouski, R. K. Dukor, X. Lu, L. A. Nafie and I. K. Lednev, *Chem. Commun.*, 2012, **48**, 2837-2839.
88. C. Sourisseau, *Chem. Rev.*, 2004, **104**, 3851-3892.
89. F. L. Labarthet, T. Buffeteau and C. Sourisseau, *Appl. Spectrosc.*, 2000, **54**, 699.
90. M. E. Rousseau, T. Lefevre, L. Beaulieu, T. Asakura and M. Pezolet, *Biomacromol.*, 2004, **5**, 2247-2257.
91. V. Sereda and I. K. Lednev, *J. Raman Spectrosc.*, 2014, **45**, 665-671.

92. D. Kurouski, S. Zaleski, F. Casadio, R. P. Van Duyne and N. C. Shah, *J. Am. Chem. Soc.*, 2014, **136**, 8677-8684.
93. M. D. Sonntag, J. M. Klingsporn, L. K. Garibay, J. M. Roberts, J. A. Dieringer, T. Seideman, K. A. Scheidt, L. Jensen, G. C. Schatz and R. P. Van Duyne, *J. Phys. Chem. C*, 2012, **116**, 478-483.
94. E. A. Pozzi, M. D. Sonntag, N. Jiang, J. M. Klingsporn, M. C. Hersam and R. P. Van Duyne, *ACS Nano*, 2013, **7**, 885-888.
95. T. Schmid, L. Opilik, C. Blum and R. Zenobi, *Angew. Chem. Int. Ed.*, 2013, **52**, 5940-5954.
96. R. Bohme, M. Mkandawire, U. Krause-Buchholz, P. Rosch, G. Rodel, J. Popp and V. Deckert, *Chem. Commun.*, 2011, **47**, 11453-11455.
97. E. M. van Schrojenstein Lantman, T. Deckert-Gaudig, A. J. Mank, V. Deckert and B. M. Weckhuysen, *Nat. Nanotech.*, 2012, **7**, 583-586.
98. B. S. Yeo, E. Amstad, T. Schmid, J. Stadler and R. Zenobi, *Small*, 2009, **5**, 952-960.
99. A. Hartschuh, E. Sánchez, X. Xie and L. Novotny, *Phys. Rev. Lett.*, 2003, **90**, 95503.
100. J. A. Dieringer, R. B. Lettan, II, K. A. Scheidt and R. P. Van Duyne, *J. Am. Chem. Soc.*, 2007, **129**, 16249-16256.
101. S. L. Kleinman, E. Ringe, N. Valley, K. L. Wustholz, E. Phillips, K. A. Scheidt, G. C. Schatz and R. P. Van Duyne, *J. Am. Chem. Soc.,* 2011, **133**, 4115-4122.
102. J. M. Klingsporn, N. Jiang, E. A. Pozzi, M. D. Sonntag, D. Chulhai, T. Seideman, L. Jensen, M. C. Hersam, and R. P. Van Duyne, *J. Am. Chem. Soc.*, 2014, **136**, 3881-3887.
103. T. Deckert-Gaudig, E. Kämmer and V. Deckert, *J. Biophoton.*, 2012, **5**, 215-219.
104. V. Deckert, T. Deckert-Gaudig, M. Diegel, I. Gotz, L. Langeluddecke, H. Schneidewind, G. Sharma, P. Singh, P. Singh, S. Trautmann, M. Zeisberger and Z. Zhang, *Faraday Discuss.*, 2015, **177**, 9-20.
105. M. D. Sonntag, D. Chulhai, T. Seideman, L. Jensen and R. P. Van Duyne, *J. Am. Chem. Soc.*, 2013, **135**, 17187-17192.
106. P. Singh, T. Deckert-Gaudig, H. Schneidewind, K. Kirsch, E. M. van Schrojenstein Lantman, B. M. Weckhuysen and V. Deckert, *Phys. Chem. Chem. Phys.*, 2015, **17**, 2991-2995.
107. M. Paulite, C. Blum, T. Schmid, L. Opilik, K. Eyer, G. C. Walker and R. Zenobi, *ACS Nano*, 2013, **7**, 911-920.
108. C. Blum, L. Opilik, J. M. Atkin, K. Braun, S. B. Kammer, V. Kravtsov, N. Kumar, S. Lemeshko, J.-F. Li, K. Luszcz, T. Maleki, A. J. Meixner, S. Minne, M. B. Raschke, B. Ren, J. Rogalski, D. Roy, B. Stephanidis, X. Wang, D. Zhang, J.-H. Zhong and R. Zenobi, *J. Raman Spectr.*, 2014, **45**, 22-31.